*sustainability*

MDPI

*Article*

# A Green Chemistry and Energy- and Cost-Effective Approach in Innovative Advanced Oxidation Processes Through Photoactive Microgels for Sustainable Applications

**Víctor Fabregat [1,2,*] and Juana María Pagán [1,*]**

[1] Department of Engineering & Innovation, Regenera Energy, C. Molina de Segura 8, 30007 Murcia, Spain
[2] Chair of Technologies for Circularity and Decarbonization, Polytechnic University of Cartagena, Campus Alfonso XIII, P.° Alfonso XIII 38, 30203 Cartagena, Spain
* Correspondence: vfabregat@regeneraenergy.es (V.F.); jmpagan@regeneraenergy.es (J.M.P.); Tel.: +34-69-3367-275 (V.F.)

**Abstract:** Current sustainability challenges for the chemical industry include developing advanced wastewater treatment technologies and transitioning to renewable biomass for more sustainable processes. This study aims to design and develop photoactive colloidal microgels for environmental applications, focusing on the removal of pollutants and the green synthesis of sustainable materials. PNIPAM-based microgels with covalently integrated Rose Bengal as a photosensitizer was synthesized and characterized. The stimuli-responsive colloidal structure of the microgels enhances substrate adsorption and reaction kinetics, surpassing free Rose Bengal due to the local concentration effect provided by the polymeric matrix at the reaction temperature and pH. These materials, designed according to green chemistry principles, enable the sustainable synthesis of 5-hydroxy-2(5H)-furanone, a C4 building block intermediate, achieving over 99% conversion in aqueous media, which is a novel aspect compared to the literature. The removal of Diclofenac from wastewater has been highly efficient, reaching degradation rates of over 99% in 160 min. The photoactive microgels act as efficient photocatalysts, validated under direct solar irradiation, capable of generating singlet oxygen ($O_2(^1\Delta g)$) with full recoverability and reusability over multiple cycles. This approach provides a cost-effective eco-friendly solution to economic and environmental challenges in water treatment, as shown by scale-up economic simulations.

**Keywords:** green chemistry; sunlight-driven photocatalysis; wastewater disinfection; C4 chemicals' sustainable synthesis; colloidal microgels; rose bengal; singlet oxygen

check for updates

Academic Editor: José Alberto Herrera-Melián

Received: 23 January 2025
Revised: 2 March 2025
Accepted: 5 March 2025
Published: 6 March 2025

**Citation:** Fabregat, V.; Pagán, J.M. A Green Chemistry and Energy- and Cost-Effective Approach in Innovative Advanced Oxidation Processes Through Photoactive Microgels for Sustainable Applications. *Sustainability* **2025**, *17*, 2331. https://doi.org/10.3390/su17052331

**Copyright:** © 2025 by the authors. Licensee MDPI, Basel, Switzerland. This article is an open access article distributed under the terms and conditions of the Creative Commons Attribution (CC BY) license (https://creativecommons.org/licenses/by/4.0/).

## 1. Introduction

At the end of the 20th century, green chemistry emerged as a discipline aimed at integrating sustainability into chemical process design, focusing on both environmental and economic aspects. Defined by P. T. Anastas and J. C. Warner through 12 guiding principles [1], it advocates for the efficient use of resources and the minimization of waste. Over time, this movement has evolved to address new challenges, highlighting the need for continued innovation in sustainable chemistry [1–4]. A relevant example is the increasing detection of Contaminants of Emerging Concern (CECs) in aquatic environments, including pharmaceuticals and endocrine disruptors, which poses a major challenge for wastewater treatment. Many CECs persist even after tertiary treatments, hindering water reuse and raising public health concerns. Research is now focused on developing advanced technologies for their effective removal and integrating these solutions into wastewater treatment plants to enhance water safety and sustainability [5–9].

In another aspect, the selection of raw materials is crucial for environmental sustainability, as it significantly impacts the process and its overall environmental footprint. Currently, 90% of organic compounds synthesized rely on raw materials derived from petroleum, which is a limited resource. The most plausible alternative is biomass, which is easily accessible, abundant, and historically provided raw materials for humanity until the advent of fossil resources [10,11]. Returning to biomass would represent a step towards closing the sustainability loop; lignocellulosic biomass is the most abundant renewable carbon source and its conversion into value-added fuels and chemicals supports sustainable energy production and carbon neutrality [10,12,13]. Among lignocellulosic biomass derivatives, furfural and furoic acid are key platform chemicals obtained through hydrolysis and oxidation processes, respectively [14,15]. Furfural was recognized by the U.S. Department of Energy as a top value-added chemical [16]. Furoic acid, readily obtained from furfural via biological oxidation, is a well-known compound in green chemistry, serving as a C4 building block intermediate for the synthesis of various industrially significant substances, including plastics, manufacturing fibers, lubricants, and resins [17–19].

On the other hand, hydrogels are extensively used in biochemistry due to their biocompatible physicochemical properties; this resemblance provides them with valuable roles in both biomedical sciences and environmental applications, particularly in water treatment and biodiversity conservation [20–22]. Poly(N-isopropylacrylamide) (PNIPAM) is one of the most widely used microgel particles due to its stimuli-responsive properties, allowing it to adapt its physical and chemical characteristics to external environmental changes. PNIPAM is a temperature-sensitive polymer, hydrophilic at room temperature, and widely used for fabricating sustainable stimuli-responsive materials with defined size, functionalized surfaces, and enhanced colloidal stability. Additional stimuli, such as pH responsiveness, can be introduced through copolymerization with ionic monomers. The swelling behavior is influenced by polymer/polymer and polymer/water interactions, as well as factors like temperature, pH, and ionic strength [23,24].

Innovative strategies are essential to drive reactions aimed at achieving biological and environmental sustainability. Within this framework, the development of polymers incorporating photosensitizing units has emerged as a topic of considerable interest. Among photocatalytic processes, oxidation remains one of the most extensively investigated. In recent years, methodologies utilizing photosensitizers have gained recognition as promising green alternatives [25–28]. Notably, singlet oxygen has demonstrated significant potential in oxidation reactions of environmental relevance, such as the synthesis of natural products and pharmaceuticals [29], as well as in pioneering applications within sustainable organic chemistry [30]. In this line, our research group has developed heterogeneous photocatalysts in the form of hydrophilic photoactive polymeric microparticles derived from styrene resins, functionalized covalently with Rose Bengal (RB) as a photosensitizer. These materials have proven effective in the photochemical oxidation of 2-furoic acid for the green synthesis of 5-hydroxy-2(5H)-furanone [17]. Moreover, they have demonstrated significant potential in removing emerging pollutants (EPs) from water through advanced oxidation processes [31,32]. The present study focuses on the covalent incorporation of RB into the PNIPAM matrix to develop a supported photosensitizer. A key advantage over previous approaches lies in the colloidal structure of the microgel, which promotes substrate adsorption under specific stimuli, such as pH and temperature, thereby enhancing the efficiency of the heterogeneous catalyst. The literature documents several instances of photosensitizers covalently bound to PNIPAM-based polymeric matrices [33–35], with Rose Bengal being utilized in some of these cases [36–41], but none of these have been applied to the specific objectives described in this article, such as the removal of Diclofenac from water and the green synthesis of raw materials from lignocellulosic biomass.

Photocatalysis, a key principle of green chemistry, is a sustainable process that uses light and a photosensitizer to drive chemical transformations. Recently, the design of polymers with photosensitizing units has gained attention. Stimuli-responsive polymers like PNIPAM, with covalently attached photosensitizing groups, allow for controlled photoreactions. This approach has been shown to effectively remove phenol from polluted water through singlet oxygen oxidation [42] and could be extended to pollutants with similar chemical structures, like Diclofenac, as demonstrated in recent studies using silica-based RB-supported photocatalysts [43,44]. To further advance the sustainable design of the photocatalytic process, another key resource is the use of renewable energy. Sunlight can be directly harnessed to induce photochemical transformations of chemical structures [45]. The sun offers immense photochemical potential, and numerous studies in the literature report the successful use of direct solar irradiation for water decontamination [46–49]. Additionally, sunlight could also be employed for the synthesis of raw materials derived from furfural [10,18].

This study introduces an innovative method for synthesizing colloidal PNIPAM microgels with covalently integrated Rose Bengal as a photosensitizer. The stimuli-responsive colloidal microgel structure enhances the photochemical efficiency of the photosensitizer by adsorbing substrates into the polymeric matrix, thereby increasing process performance. The novelty of this study lies in the design and composition of the polymeric structure, its direct validation under direct solar irradiation as an advanced oxidation process driven by singlet oxygen, targeting applications in pollutant degradation and green synthesis, the latter enabling its execution in an aqueous medium. The polymer's design aligns with green chemistry principles, and its intended uses include sustainable goals such as synthesizing 5-hydroxy-2(5H)-furanone as a renewable raw material and removing CECs, such as Diclofenac, from wastewater. The approach integrates cost-effective and sustainable strategies, including light-driven photocatalysis using solar energy, recyclability with straightforward material separation (heterogeneous catalysis), the non-use of organic solvents, minimal energy requirements (solar light and ambient temperature reactions), and reduced byproduct generation. This makes the microgels an eco-friendly and efficient solution for environmental challenges.

## 2. Materials and Methods

### *2.1. Reagents, Solvents, and Polymeric Precursors*

The reagents used in the present work are listed below: N-isopropylacrylamide (NIPAM, Fisher, Waltham, MA, USA, purified by recrystallization with hexane/toluene), aminoethyl methacrylate (AEMA, Aldrich, Seelze, Germany, 90%), N,N′-methylenebisacrylamide (MBAM, Fisher, purified by recrystallization from ethanol), 2,2′-azobis[2-(methylamidinopropane)] dichloride (V50, Aldrich, 97%), hydrochloric acid (HCl, Scharlau, Barcelona, Spain, extra pure, 37%), Rose Bengal sodium salt (RB, Fluka, Buchs, Switzerland), chloroform ($CHCl_3$, Scharlau, stabilized with ethanol, multisolvent grade for HPLC), 1-[3-(dimethylamino)propyl]-3-ethylcarbodiimide (EDC, Aldrich), methanol (MeOH, Scharlau, multisolvent grade for HPLC), 9,10-anthracenedipropionic acid (ADPA, Aldrich, ≥98.0%), Diclofenac (Sigma, Burlington, MA, USA), and furoic acid (Sigma). The water used in all cases was of Millipore–Q quality (Milli-Q, Burlington, MA, USA, ultrapure, double-deionized).

### *2.2. Synthesis of the Photoactive Colloidal Microgels*

Step 1. Synthesis of NIPAM-co-AEMA polymeric microgel

The synthesis of NIPAM-co-AEMA microgels was performed via single-step emulsion polymerization in a 100 mL reaction vessel equipped with a reflux condenser, magnetic stirrer, thermometer, and an argon gas inlet. NIPAM (0.99 g, 99 wt.% of the total monomer),

AEMA (0.01 g, 1 wt.%), and MBAM (0.10 g, 10 wt.% as the crosslinker) were dissolved in 100 mL of Milli-Q water and added to the reaction vessel. The mixture was heated in an oil bath maintained at 70 °C and purged with argon gas for 20 min to remove oxygen. After the system reached the target temperature, a solution of the initiator (0.04 g of V50, 4 wt.% of the total monomer weight) in 5 mL of Milli-Q water was introduced into the vessel. The polymerization was carried out for 24 h under constant stirring. Upon completion, the reaction mixture was cooled to room temperature, and the resulting microgel dispersion was dialyzed against Milli-Q water for a week to remove unreacted monomers and other impurities, with the dialysate replaced daily.

Step 2. Rose Bengal anchorage via carbodiimide coupling reaction: synthesis of NIPAM-co-AEMA-RB

Rose Bengal sodium salt was dissolved in water and acidified to pH = 2 using 1 M HCl. The resulting solution was extracted with chloroform, and the organic phase was washed three times with water to remove impurities. The product was then concentrated under reduced pressure. In a 100 mL round-bottomed flask, NIPAM-co-AEMA polymer (1.412 g, $8.52 \times 10^{-5}$ mol AEMA), acidified Rose Bengal (83 mg, $8.52 \times 10^{-5}$ mol), and 1-ethyl-3-(3-dimethylaminopropyl)carbodiimide (EDC) (1.6 mg, $8.52 \times 10^{-6}$ mol) were combined. Methanol was added as the solvent to a final volume of 100 mL. The flask was sealed with a septum and the mixture was stirred at room temperature for 48 h to allow the covalent attachment of Rose Bengal to the polymer. After the reaction, the microgel particles were separated by centrifugation at 10,000 rpm for 20 min using a Sorvall RC 5b Plus centrifuge. The particles were washed sequentially with methanol, a 1:1 methanol–water solution, and, finally, with water to ensure the removal of unreacted reagents. The supernatant from the washing steps was collected to quantify the Rose Bengal loading via UV-Vis spectroscopy. Finally, the purified microgel particles were dispersed and stored in 100 mL of Milli-Q water.

### *2.3. Characterization of the Colloidal Microgels*

The characterization process of the colloidal polymeric microgels was performed using acid-base titration experiments, dynamic light scattering (DLS), and UV-Vis absorption spectroscopy. Acid-base titration via potentiometry was conducted with a Crison Titromatic potentiometric titration instrument. When required, the pH was adjusted by adding small quantities of 0.01 M HCl or 0.01 M NaOH. These experiments enabled the quantification of the AEMA percentage in the NIPAM-co-AEMA microgel particles (by analyzing the $NH_2$ group of this monomer, which protonates in an acidic medium). Additionally, the yield of the overall reaction was determined by acid-base titration, quantifying the amount of RB anchored to the polymer NIPAM-co-AEMA-RB. The natural pH of each microgel was also measured.

Dynamic light scattering (DLS) analysis was performed to study the colloidal properties of the polymers. These studies were conducted using a Brookhaven Zeta-Plus (laser 15 mW, $\lambda_{em}$ = 678 nm, detector 90°). This technique allows for determining the diffusion coefficients of the colloidal microgels and their electrophoretic mobility. All samples were prepared at a particle concentration of 0.1% by weight in Milli-Q water and placed in a 3 mL quartz cuvette. The diffusion coefficients of the microgel particles were used to calculate their hydrodynamic diameter using the Stokes–Einstein equation. UV-Vis absorption spectroscopy studies were carried out using a Hewlett-Packard Agilent 8453 UV-Vis spectrophotometer. The calculation of RB loading after the covalent attachment of Rose Bengal to the NIPAM-co-AEMA polymer was performed by two methods: acid-base titration (as described previously) and UV-Vis spectroscopy (λ = 549 nm), analyzing the unreacted RB in the supernatant and comparing both results.

The adsorption capacity of the microgels was characterized through experiments with different substrates. The chosen substrates were those intended for subsequent photochemical studies in this work (ADPA, Diclofenac, and furoic acid). These experiments also served to determine the optimal ratio between substrate concentration and hydrogel weight for each reaction. To achieve this, several solutions containing a fixed amount of microgel particles were mixed with a known and variable amount of substrate in Milli-Q water, and the system was left to equilibrate for 24 h. The particles were then separated from the solution by centrifugation (10,000 rpm for 20 min, using a Sorvall RC 5B Plus centrifuge). The experiment was performed at the natural pH of the microgel. In cases where deviations occurred after the substrate was added, the pH was adjusted by adding small quantities of 0.01 M HCl or 0.01 M NaOH. UV-Vis spectroscopy measurements were performed in order to evaluate the adsorption of the substrates ADPA (UV-Vis Hewlett-Packard Agilent 8453 at 398 nm) and furoic acid (246 nm) into the microgel. For Diclofenac, the measurements were performed using HPLC (Agilent 1260 with 4-nitrobenzoic acid $10^{-4}$ M). For each case, curves of μmol substrate per gram of microgel as a function of the equilibrium substrate concentration were plotted.

### *2.4. Evaluation the Photo-Oxidation Kinetics of the Photoactive Colloidal Microgels*

The singlet oxygen production efficiency of the polymeric microgel photosensitizers was evaluated using the standard photo-oxidation reaction of anthracene-9,10-dipropionic acid (ADPA), a method previously reported in the literature [17,31,50]. The experiments were conducted in aqueous media within a 500 mL jacketed Pyrex reactor (Proquilab, Cartagena, Spain) containing ADPA at a concentration of $1.2 \times 10^{-4}$ M in Milli-Q water. The required amount of microgel solution was added based on the adsorption data obtained in adsorption experiments. The pH of the solution was measured, and if it deviated from the natural pH of the microgel, it was adjusted using small volumes of 0.01 M HCl or 0.01 M NaOH.

In the first experimental phase, the air-equilibrated solution was irradiated at 25 °C using a 50 W halogen lamp, with continuous stirring throughout the process. The jacketed part of the reactor was filled with an aqueous $FeCl_3$ solution (0.1 M), serving as a filter for wavelengths below 450 nm. The temperature was monitored to ensure it remained within the range of 23–25 °C. The jacketed $FeCl_3$ solution was connected to a water flow system linked to a small heater/cooler to regulate the temperature if needed. At regular intervals, a 3 mL aliquot was withdrawn using a $1 \times 1$ cm quartz spectrophotometer cuvette to monitor the decreasing absorbance of ADPA. Reaction kinetics were calculated using the kinetics mode of a Hewlett-Packard Agilent 8453 UV-Vis spectrophotometer at 398 nm, employing the same reaction cuvette. In order to compare the effect of the microgel, similar experiments were conducted without the microgel, using only an RB solution at a concentration equivalent to that of the RB covalently anchored to the microgel. Control experiments without irradiation were also performed.

The second phase of experiments was conducted under direct natural solar irradiation. The reactor was set up following the same protocol as in the previous experiment, with the only modification being the change in the irradiation source from artificial to natural sunlight. The irradiation at the surface of the reaction medium was measured using a Fluke IRR1-SOL meter, the temperature was monitored to ensure it remained within range, and the ADPA concentration was measured using UV-Vis spectroscopy.

### *2.5. Studies of Diclofenac Pollutant Photo-Degradation*

To evaluate the degradation of the Diclofenac pollutant, experiments were conducted following the same protocol as before for irradiation with both simulated solar light

(50 W halogen lamp) and natural sunlight. In both cases, a 500 mL jacketed reactor system surrounded by an $FeCl_3$ solution was used. The appropriate amount of microgel, determined from adsorption studies, was added to a 5 ppm ($1.69 \times 10^{-5}$ M) Diclofenac solution in Milli-Q water. The pH was also adjusted to the natural pH of the microgel and, under continuous stirring, the temperature was maintained at 25 °C using the previously described system. The photo-oxidation reaction of the pollutant Diclofenac was monitored by analyzing 200 μL aliquots taken at known time intervals using Agilent 1260 reversed-phase HPLC chromatography. A $10^{-4}$ M solution of 4-nitrobenzoic acid was used as an internal standard, with the temperature maintained at 30 °C.

Control experiments were also conducted under identical conditions without a photosensitizer, as well as with a Rose Bengal solution at a concentration equivalent to the amount of RB anchored to the microgel, serving as the photosensitizer. The impact of solar irradiation was evaluated using both simulated sunlight (50 W halogen lamp) and natural sunlight. For the natural sunlight experiments, the setup was exposed to direct sunlight on sunny days in Murcia during midday hours at various times of the year to account for seasonal variations in solar irradiation. In all experiments, the solar irradiation at the surface of the reaction medium was measured using a Fluke IRR1-SOL meter, and the temperature was carefully monitored to ensure it remained between 23 and 25 °C.

The recyclability of the NIPAM-co-AEMA-RB photosensitizer was assessed through a series of photo-catalytic experiments. The procedure followed was identical to the previously described method, with the Diclofenac solution being renewed for each cycle. Each reaction cycle was conducted for 180 min, with cycle 2 performed without irradiation as a control. At the end of each cycle, the microgel photocatalysts were recovered from the solution by centrifugation at 10,000 rpm for 20 min using a Sorvall RC 5B Plus centrifuge (Sorvall, Waltham, MA, USA).

### *2.6. Photo-Oxidation of Furoic Acid and Green Synthesis of 5-Hydroxy-2(5H)-Furanone*

The oxidation of 2-furoic acid to 5-hydroxy-2(5H)-furanone via singlet oxygen was studied in an aqueous reaction medium (Milli-Q water with methanol 95:5 $v/v$). The appropriate amount of microgel photosensitizer was added to 500 mL of a 2-furoic acid solution ($10^{-3}$ M) in a jacketed Pyrex reactor. The heterogeneous mixture was maintained under stirring and in equilibrium with air. Subsequently, the experiments were conducted following the same protocol as previously described for irradiation with both simulated sunlight (50 W halogen lamp) and natural sunlight (at different times of the year) while monitoring the incident irradiation. The pH was adjusted to the natural pH of the microgel, and the temperature was kept between 23 and 25 °C under stirring, using the previously described procedure. Control experiments were conducted under identical conditions in the dark, with free Rose Bengal in solution as the photosensitizer (at the same concentration as the RB anchored in the microgel). The decreasing absorbance of 2-furoic acid was monitored by UV–Vis spectroscopy at 246 nm. For each measurement, 3 mL aliquots were withdrawn from the reaction mixture and analyzed using a quartz spectrophotometer cuvette, following the same procedure as with ADPA. After the reaction was completed, the photocatalyst was recovered by centrifugation (10,000 rpm for 12 min, using a Sorvall RC 5B Plus centrifuge), and the product was analyzed by HPLC to confirm the successful synthesis of 5-hydroxy-2(5H)-furanone and the absence of reactants or byproducts, such as additional oxidation to maleic acid or others. The catalyst was then reused to evaluate its catalytic efficiency across multiple reaction cycles.

## 3. Results and Discussion

### *3.1. Synthesis and Characterization of the Photoactive Colloidal Microgels*

The microgels were designed following green chemistry principles and in order to incorporate energy efficiency into their future functional use. The polymeric matrix was formulated with 90% of N-isopropylacrylamide (NIPAM), 1% of aminoethylmethacrylate (AEMA)—a total of 91% monomer—and 9% of methylenbisacrylamida (MBAM) as a crosslinker, leveraging the pH- and temperature-responsive properties of NIPAM for controlled swelling with enhanced substrate adsorption and increased reaction efficiency. This design enables reactions to occur in water without organic solvents, aligning with green chemistry goals. Additionally, the microgels' natural pH matches that of wastewater treatment plant effluents, making them suitable for quaternary water treatment to remove CECs. Furthermore, PNIPAM microgels are non-toxic per Regulation (EC) No. 1272/2008, ensuring environmental and human safety. As discussed in the introduction, previous studies have synthesized copolymers with other monomers anchored to PNIPAM [23,36]. In this design, AEMA was selected as the co-monomer and incorporated in a small proportion (90:1 ratio relative to NIPAM); the amount of AEMA determines the RB loading. The selection of the 90:1 ratio is sufficient to ensure the effective anchoring of RB for efficient sunlight-driven photocatalysis [17,31,32] while minimizing the presence of unreacted $-NH_2$ groups that could interfere with the microgel's properties. Additionally, this proportion helps maintain cost-effectiveness, considering the higher price of RB compared to the monomers. The colloidal structure of the PNIPAM-based microgel with covalently anchored RB enhances the photocatalytic properties of free RB by promoting substrate adsorption within the polymeric matrix. At a specific pH and temperature, the microgel facilitates substrate concentration, creating a localized environment that increases reaction efficiency. This local concentration effect improves singlet oxygen generation and overall photocatalytic performance, surpassing that of free RB in solution.

The 9% MBAM crosslinker enhances the microgel's substrate adsorption capacity by providing porosity, flexibility, and permeability to the polymeric structure, with this proportion optimized based on previous studies [51–54]. Furthermore, the green design of the microgels includes a PNIPAM-based matrix with near 100% polymerization efficiency, minimizing waste during synthesis. Its functional applications include photocatalysis under sunlight, water as the reaction solvent, and the ability to be reused across multiple reaction cycles, all aligning with green chemistry principles.

The colloidal aqueous microgels were synthesized in two steps. The polymer synthesis involved an initial polymerization step, as previously described in the literature [55,56], in which NIPAM-co-AEMA microgels were synthesized by copolymerizing NIPAM and AEMA with MBAM as the crosslinker. As shown in Figure 1, the polymer resulting from the first reaction step, NIPAM-co-AEMA (without RB attached), exhibits a white color. In a second step, the photosensitizer Rose Bengal is covalently attached within the polymeric matrix through a carbodiimide coupling reaction (Figure 2) [57]. The polymer NIPAM-co-AEMA-RB has the appearance of colloidal solution and displays a pink hue due to the covalently attached RB.

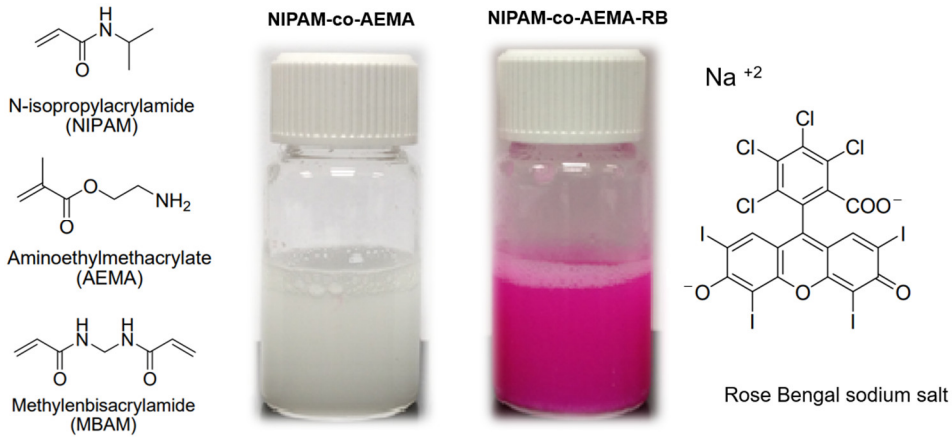


**Figure 1.** (**Left**) Chemical structure of NIPAM, AEMA, and MBAM. Centre: Illustration of colloidal microgels without RB (left vial, NIPAM-co-AEMA) and with covalently anchored Rose Bengal (NIPAM-co-AEMA-RB). (**Right**) Chemical structure of Rose Bengal in basic media $RB^{-2}$.

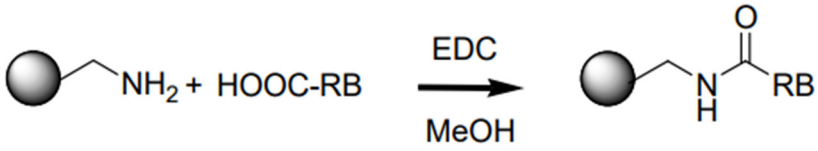


**Figure 2.** Scheme of the carbodiimide coupling reaction in MeOH medium using EDC and Rose Bengal with the carboxylate group protonated (HOOC-RB, previously adjusted to pH = 2).

The new microgels were characterized, and the colloidal properties of the polymers were studied. These studies included acid-base titration experiments, diffusion coefficients, electrophoretic mobility, and UV-Vis spectroscopy analysis, as described in the previous section. Due to the colloidal nature of the polymer particles, the study of a suitable polymerization process for the monomers and crosslinkers could not be conducted using conventional methods like FT-IR spectroscopy and FT-Raman spectroscopy, which have been employed in previous studies [17,51–54]. Instead, experiments of acid-base titration of the polymers were performed. The variation in the pH was accomplished in order to study the dependence of NIPAM-co-AEMA colloidal microgels to the external stimulus pH, analyzing the $NH_2$ group of AEMA. The results indicate that the polymerization reaction was successful, as the AEMA percentage obtained by titration closely matches the theoretical value (0.91%). Table 1 summarizes the results obtained for the characterization of the two synthesized polymers in terms of effective diameter and electrophoretic mobility (determined by DLS analysis) as well as the AEMA composition (acid-base titration).

Table 1 shows the natural pH values of the hydrogels: 6.69 for NIPAM-co-AEMA and 6.45 for NIPAM-co-AEMA-RB. These results are consistent with expectations, as the natural pH of PNIPAM in pure water is close to 7. The slightly lower experimental values in both cases are due to the mild acidity introduced by the functional groups in the polymeric network contributed by the ≅1% AEMA comonomer. That is, the amino group exclusively for NIPAM-co-AEMA and the non-functionalized amino group along with the Rose Bengal for NIPAM-co-AEMA-RB. Indeed, the optimal pH range for substrate adsorption in the microgels aligns with their natural pH of within the slightly acidic range (pH 6–7).

**Table 1.** Effective diameter and electrophoretic mobility in different pHs for colloidal microgels.

| Characterization Data | | NIPAM-co-AEMA | NIPAM-co-AEMA-RB |
|---|---|---|---|
| Effective diameter (nm) | pH = 3 | 732 | 724 |
| | Natural pH of microgel | 655 | 669 |
| | pH = 7 | 631 | 634 |
| | pH = 11 | 488 | 498 |
| Electrophoretic mobility ($m^2s^{-1}V^{-1}$) | pH = 3 | 0.15 | 0.18 |
| | Natural pH of microgel | 0.02 | 0.07 |
| | pH = 7 | 0.01 | 0.03 |
| | pH = 11 | −0.09 | −0.32 |
| % AEMA (titration) | | 0.92% | 0.92% |
| RB loading (titration) | | 0 | 33 μmol RB/g polym. |
| RB loading (UV-Vis) | | 0 | 33 μmol RB/g polym. |

On the other hand, a dependence of the effective diameter and electrophoretic mobility on pH can be observed. The effective diameter of the microgels is larger in acidic pH due to increased swelling caused by electrostatic repulsion from the positive charges contributed by AEMA. As the pH increases, the effective diameter decreases, indicating a gradual contraction of the polymeric network. At the natural pH of the microgels, which is near neutral, the structure achieves its most balanced state between swelling and contraction, promoting optimal substrate adsorption within this pH range. Regarding electrophoretic mobility, both microgels display positive values at acidic pH, near zero at neutral pH, and negative values at basic pH. In the case of NIPAM-co-AEMA-RB, the mobility values are more pronounced compared to NIPAM-co-AEMA, particularly at acidic and basic pH. This heightened response is due to the amino groups from AEMA contributing to positive mobility at acidic pH and the negatively charged groups from Rose Bengal dominating at basic pH. For uncharged pollutants, which are most common, natural microgel pH or neutral pH with low electrophoretic mobility enhance adsorption.

The zeta potential ($\zeta$) can be calculated from the electrophoretic mobility ($\mu$) by means of the Hückle equation: $\mu = 2\varepsilon\zeta/3\eta$ (where $\varepsilon$ is the permittivity and $\eta$ is the viscosity of the medium, in this case, water). At pH~6–7, the microgel remains in a moderate swelling state, optimizing the porosity and surface area for adsorption. In this operational pH, both $\mu$ ($m^2s^{-1}V^{-1}$) and $\zeta$ (mV) are close to 0, and this provides an optimal balance between electrostatic interactions, swelling behavior, and hydrophobic affinity, making it highly favorable for substrate adsorption and subsequent photocatalytic or degradation processes. On the other hand, the optimum temperature for the best adsorption of PNIPAM microgels is between 23 and 25 °C [36].

The particle size of the polymeric microgels was determined using dynamic light scattering, with the effective diameter calculated from diffusion coefficients using the Stokes–Einstein equation: $D = kT/(6\pi\eta R)$. This equation relates the diffusion coefficient (D) to the particle radius (R), accounting for temperature (25 °C, in this study), the Boltzmann constant (k), and the solvent viscosity (water, in this study) [58].

Regarding the calculation of RB loading in NIPAM-co-AEMA-RB using the acid-base titration method, the carboxylate group of RB is the one that binds to the amino group through the carbodiimide coupling reaction. However, under basic pH conditions, RB can lose a proton from its hydroxyl group; the value obtained using this method is 33 μmol RB/g microgel, as presented in Table 1. Moreover, as mentioned in the methodology section, the amount of Rose Bengal covalently attached to NIPAM-co-AEMA-RB was also calculated by analyzing the unreacted supernatant after prior calibration using UV-Vis spectroscopy ($\lambda$ = 549 nm). The acquired value was 33 μmol RB/g microgel, which is the

same result obtained using the acid-base titration method. All results of the titration studies can be found in the Supplementary Materials.

Finally, adsorption studies (Figure 3) were conducted to evaluate the adsorption capacity of microgel NIPAM-co-AEMA-RB using three different substrates (ADPA, Diclofenac, and furoic acid), which will be employed in subsequent experiments. These studies not only validated the microgels' ability to adsorb the substrates, but also determined the optimal microgel-to-substrate ratio required for effective adsorption in the medium.

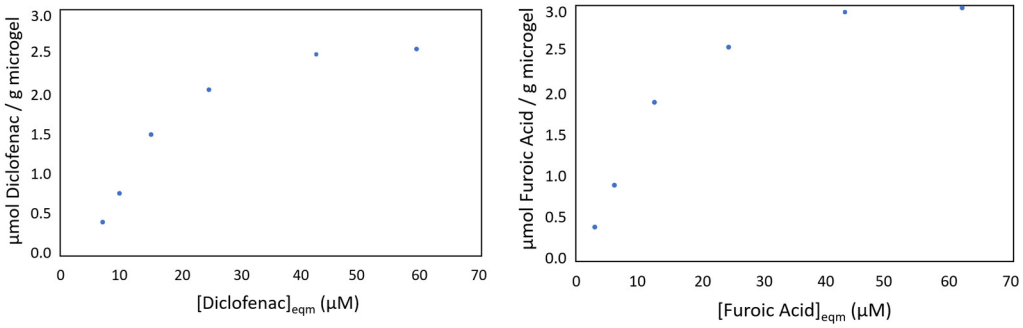


**Figure 3.** Graphics of substrate adsorption in the microgel NIPAM-co-AEMA-RB (Diclofenac, (**left**) and furoic acid, (**right**)) in µmol substrate/g microgel as a function of the equilibrium substrate concentration at 25 °C and pH = 6.45.

The results obtained were 0.69 µmol ADPA/g microgel, 2.55 µmol Diclofenac/g microgel, and 3.01 µmol furoic acid/g microgel. The highest adsorption was observed for furoic acid, while the lowest was for ADPA, with a difference of half an order of magnitude. This difference is attributed to their chemical properties: furoic acid is smaller, has a single carboxyl group, and its furan ring facilitates effective electrostatic and hydrophobic interactions with the protonated amino groups of the microgel, especially at a slightly acidic or neutral pH. In contrast, ADPA, being larger and bearing two carboxylate groups, experiences greater charge repulsion, limiting its adsorption. Diclofenac, with an intermediate molecular weight and a single carboxyl group that remains deprotonated at a slightly acidic pH, also interacts effectively with the microgel, resulting in adsorption values slightly lower than furoic acid but higher than ADPA.

### *3.2. Evaluation the Photo-Oxidation Kinetics of the Photoactive Colloidal Microgels*

The production efficiency of singlet oxygen by the polymeric photosensitizers was evaluated using the standard photo-oxidation reaction of anthracene-9,10-dipropionic acid (ADPA). In this process, ADPA reacts with $O_2(^1\Delta_g)$, forming ADPA endoperoxide. The photo-oxidation experiments were conducted as outlined in Section 2.4, using 86.95 mg of microgel added to a solution of $1.2 \times 10^{-4}$ M ADPA in Milli-Q water. The reactions were performed in a 500 mL jacketed reactor surrounded by the $FeCl_3$ ($\lambda < 450$ nm filter) solution under constant stirring and equilibrated with air. The temperature control system was activated to maintain the reaction temperature between 23 °C and 25 °C. At regular intervals, 3 mL aliquots were collected and analyzed in a quartz spectrophotometer cuvette, monitoring the decrease in the ADPA absorption band at 398 nm. The experiments were performed using two different irradiation sources: (1) a 50 W halogen lamp and (2) natural sunlight. The irradiation at the surface of the reaction medium was measured. For the halogen lamp experiments, the vials were positioned at a distance where the lamp's emission matched the average natural irradiation of that in the solar experiments. To evaluate the effect of the microgel, comparable experiments were carried out without the microgel, using only Rose Bengal at a concentration equivalent to that of the covalently anchored RB in the microgel, specifically $5.74 \times 10^{-3}$ M. Control experiments without

irradiation were also performed, with no decrease observed in the ADPA absorption band. Table 2 summarizes the study on ADPA conversion, including the reaction rate constants ($k_{obs}$) and a comparison between the different irradiation sources and the performance of microgel-anchored RB versus free RB. In all cases, the decrease in ADPA concentration follows first-order kinetics, according to the literature [17,31,32,50].

**Table 2.** Kinetic parameters ($k_{obs}$, half-reaction time and time for >99% conversion) for ADPA conversion under different irradiation sources and comparison of microgel-anchored RB vs. free RB.

| Photosensitizer | | t ½ (s) | t (>99%) (s) | $k_{obs}$ ($10^{-5}$ $s^{-1}$) |
|---|---|---|---|---|
| Halogen lamp (sun-simulated) | Blank | - | - | - |
| | NIPAM-co-AEMA | - | - | - |
| | NIPAM-co-AEMA-RB | 170 | 1128 | 408 |
| | Free RB | 200 | 1332 | 346 |
| Sun: natural irradiation (May 2024) | Blank | - | - | - |
| | NIPAM-co-AEMA | - | - | - |
| | NIPAM-co-AEMA-RB | 171 | 1135 | 406 |
| | Free RB | 204 | 1357 | 339 |

The average solar irradiation in both experiments (halogen lamp and natural solar light) was 6.9 kWh/$m^2$, aligning with expected values for May sunlight in Murcia [59]. The reaction temperature remained consistently between 24 and 25 °C, with no use of the temperature control system; this was due to the short reaction times and the initial temperature of the Milli-Q water being 25 °C, contributing to the overall energy efficiency of the process. The key findings are that microgel NIPAM-co-AEMA-RB effectively generates singlet oxygen with equivalent efficiency under both sunlight and laboratory conditions when exposed to identical irradiation levels. Additionally, the kinetic parameters of RB anchored in the microgel surpass those of free RB, as illustrated in Figure 4. This enhancement is attributed to the local concentration effect caused by the substrate adsorption onto the stimuli-responsive colloidal structure of the PNIPAM polymeric matrix [23,36], as illustrated in Figure 4b.

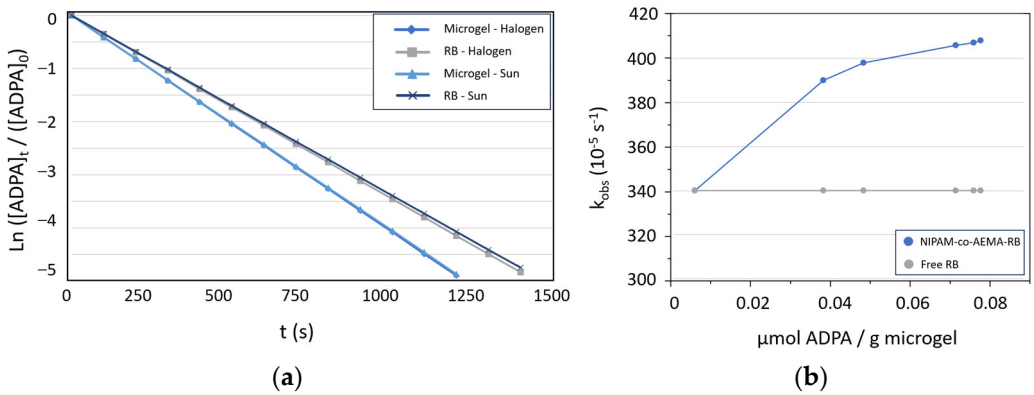


(**a**) (**b**)

**Figure 4.** (**a**) Comparison of first-order kinetic parameters for singlet oxygen production between microgel-anchored RB and free RB. (**b**) Evolution graph of reaction rates of the microgel NIPAM-co-AEMA-RB vs. substrate (ADPA) adsorption onto the microgel. Comparison with free Rose Bengal, which remains constant.

### *3.3. Studies of Diclofenac Pollutant Photo-Degradation*

The degradation capacity of the NIPAM-co-AEMA-RB microgel for the pollutant Diclofenac was investigated, following a similar approach to the ADPA studies. Experiments were conducted as described in Section 2.5, under both 50 W halogen lamp irradiation

and natural solar irradiation conditions. For the latter, experiments were performed at different times of the year to assess the impact of seasonal sunlight variations. In both setups, the irradiation on the surface of the 500 mL jacketed reactor was monitored, and the temperature was controlled to remain within the range of 23–25 °C. The jacketed section of the reactor was filled with the filter solution for wavelengths below 450 nm, preventing the direct photo-degradation of RB, the microgels, and Diclofenac. Inside the reactor, 3.31 g of microgel was added to a 5 ppm Diclofenac solution. For control experiments with free RB, the dye solution concentration was adjusted to $2.2 \times 10^{-4}$ M, equivalent to the amount of RB anchored to the microgel. Table 3 presents the results, demonstrating that both NIPAM-co-AEMA-RB and free RB achieved the complete degradation of Diclofenac within approximately 3 h of reaction.

**Table 3.** Measured solar irradiation values and kinetic parameters ($k_{obs}$ and time for >99% conversion) for Diclofenac degradation conversion under different irradiation scenarios.

| Photosensitizer | | Solar Irradiation (kWh/m$^2$) | t (>99%) (min) | $k_{obs}$ (min$^{-1}$) |
|---|---|---|---|---|
| Halogen lamp (sun-simulated) | Blank | 6.9 | - | - |
| | NIPAM-co-AEMA | | - | - |
| | NIPAM-co-AEMA-RB | | 164 | 0.02808 |
| | RB | | 182 | 0.02530 |
| Sun: natural irradiation June | Blank | 7.2 | - | - |
| | NIPAM-co-AEMA | | - | - |
| | NIPAM-co-AEMA-RB | | 165 | 0.02791 |
| | RB | | 181 | 0.02544 |
| Sun: natural irradiation September | Blank | 6.1 | - | - |
| | NIPAM-co-AEMA | | - | - |
| | NIPAM-co-AEMA-RB | | 165 | 0.02788 |
| | RB | | 184 | 0.02532 |
| Sun: natural irradiation December | Blank | 3.3 | - | - |
| | NIPAM-co-AEMA | | - | - |
| | NIPAM-co-AEMA-RB | | 169 | 0.02725 |
| | RB | | 188 | 0.02450 |

The reaction kinetics followed a first-order model in all cases, with half-life times of around 24–25 min for NIPAM-co-AEMA-RB and 27–28 min for free RB (Figure 5a). No degradation of RB, either free or supported on the microgel, was detected during the experiments under either direct sunlight or simulated solar irradiation. Moreover, as observed previously, the supported dye in the microgel exhibited better reaction kinetics than free RB, with a clear local concentration effect due to substrate adsorption. As shown in Figure 5b, the NIPAM-co-AEMA-RB microgel displays a progressive increase in the observed rate constant as Diclofenac adsorption onto the microgel increases. Additionally, an experiment was conducted under the same conditions using $TiO_2$ as a heterogeneous photocatalyst at a concentration of $2.2 \times 10^{-4}$ M (identical to that of free RB and RB anchored to the microgel). Both free RB and $TiO_2$ maintained a stable and lower kinetic constant than the microgel, indicating that adsorption onto the microgel enhances process efficiency compared to the free molecule in solution.

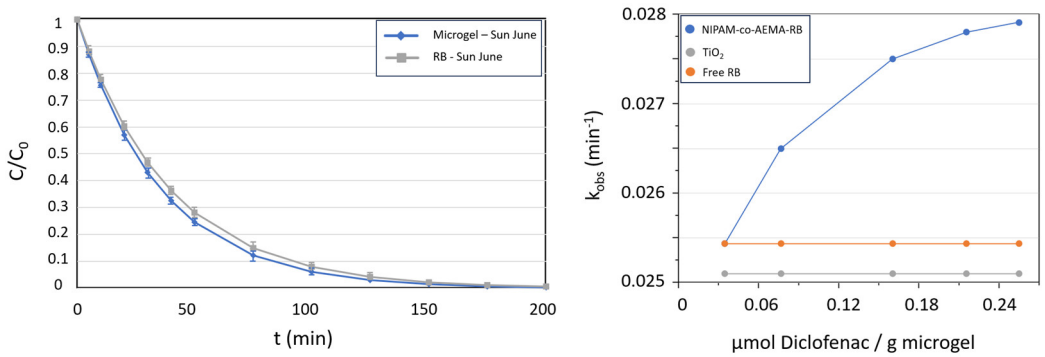


(**a**) (**b**)

**Figure 5.** (**a**) Degradation ratio of Diclofenac over time (C) relative to the initial concentration ($C_0$) for free RB and NIPAM-co-AEMA-RB in triplicate-performed experiments carried out in June. (**b**) Evolution graph of Diclofenac adsorption onto the NIPAM-co-AEMA-RB microgel vs. reaction rates of the microgel. Comparison with free Rose Bengal and $TiO_2$, both at a concentration of $2.2 \times 10^{-4}$ M and remaining constant.

An analysis of the seasonal variation experiments indicates that the expected changes in solar irradiation had no impact on the reaction kinetics. This consistency can be attributed to the design of the microgels, which include a sufficient amount of RB to produce singlet oxygen even during periods of reduced solar irradiation [32]. Regarding temperature control, the average recorded temperatures across all experiments, including those with the halogen lamp, were consistently between 23 °C and 25 °C. The thermostat system in the jacketed reactor was used minimally, except during the experiments conducted in December. In the summer experiments, the initial temperature was 23 °C, which naturally increased to 25 °C without the need for cooling. During the winter experiments, the starting temperature was set at 25 °C, and the heating system was only activated if the temperature dropped below 23.5 °C. The experiments conducted in September and those with the halogen lamp required almost no use of the thermostat system, as the external temperature during these reactions was close to the desired range.

Previous studies have reported that heterogeneous catalysis offers the advantage of preventing dye degradation, a phenomenon observed for free RB during Diclofenac degradation in recent works [43,44]. Likely, the filter used in this design helped prevent the degradation of free RB; however, the primary goal is to ensure that the supported photocatalyst remains stable and active over multiple cycles.

Recyclability studies of the NIPAM-co-AEMA-RB photosensitizer were conducted by recovering the photocatalyst via centrifugation and replacing the Diclofenac solution after each cycle. The results were remarkable, with the microgel maintaining its kinetic properties over 40 consecutive cycles without any loss in activity. This limit of 40 cycles was chosen for experimental proof-of-concept purposes and not because of observed performance degradation. In fact, the catalytic regeneration potential is much higher, as the NIPAM-co-AEMA-RB microgel demonstrated recyclability for up to 100 cycles in the photo-oxidation of ADPA without losing activity (ADPA experiments involved more cycles due to shorter degradation times compared to Diclofenac). These findings confirm that the new colloidal microgels can function as efficient and robust photocatalysts for a large number of reaction cycles.

Figure 6 presents an interpretation of the photocatalytic mechanism for the photo-oxidation of Diclofenac. Upon visible light absorption (500–600 nm), Rose Bengal transitions to its excited singlet state (RB*), generating singlet oxygen ($O_2(^1\Delta g)$) from ground-state molecular oxygen ($O_2(^3\sum g)$). Then, it interacts with Diclofenac via charge transfer, acquiring a partial negative charge while inducing a partial positive charge on Diclofenac. If

the interaction is effective, Diclofenac undergoes sequential oxidation by singlet oxygen, potentially leading to complete mineralization. However, as shown in the lower part of the diagram, quenching is not always fully efficient, and both compounds may return to their initial state. HPLC analysis of the supernatant after Diclofenac degradation revealed no intermediate products such as nitroxides, quinones, or chlorophenols. This suggests that the ring opening of the contaminant via photo-oxidation was successful. The aromatic rings likely underwent rapid cleavage, directly forming smaller aliphatic compounds (e.g., oxalic acid, formic acid) instead of accumulating as aromatic intermediates. Complete mineralization cannot be confirmed, as some degradation products (e.g., small organic acids) may be undetectable by HPLC. Future studies assessing Diclofenac degradation in real wastewater effluents will address this using LC-MS or IC (Ion Chromatography) to identify low-molecular-weight carboxylic acids and inorganic ions such as $Cl^-$ and $NO_3{}^-$. Finally, it is worth noting that, in both ADPA and Diclofenac experiments, the kinetics suggest degradation via singlet oxygen photocatalysis [17,31,32]. However, in the case of Diclofenac photo-degradation, the involvement of other reactive species cannot be entirely ruled out, although, in this case, the reaction kinetics strongly indicate that singlet oxygen is the main driver of the oxidation process. As supported by previous studies [43,44], reactive species such as •OH radicals may contribute to the mineralization of Diclofenac during later stages of degradation following singlet oxygen activity. Nevertheless, this proof-of-concept study aims to demonstrate the sustainable effectiveness of the newly designed green materials in removing contaminants.

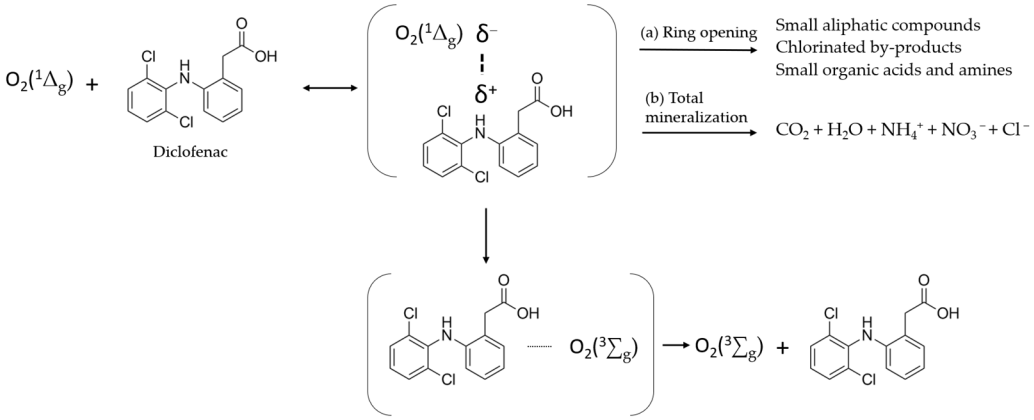


**Figure 6.** Quenching of singlet molecular oxygen $O_2(^1\Delta_g)$ by Diclofenac.

### *3.4. Studies of Photo-Oxidation of Furoic Acid and Green Synthesis of 5-Hydroxy-2(5H)-Furanone*

The green synthesis of 5-hydroxy-2(5H)-furanone was performed using singlet oxygen following the same protocol as with the previous substrates. For this reaction, 166.11 mg of microgel was added to a 500 mL jacketed reactor containing a $10^{-3}$ M solution of 2-furoic acid in Milli-Q water with 5% methanol (95:5 *v*/*v*). The pH was adjusted to match the natural pH of the microgel due to the slight acidification of the medium. The jacketed section of the reactor was filled with an $FeCl_3$ solution, which acted as a filter for wavelengths below 450 nm and as a temperature regulator. The reaction was carried out under continuous stirring and aeration, with temperature monitored and controlled, and irradiation at the surface of the reaction medium recorded. The synthesis was performed under both simulated sunlight (using a 50 W halogen lamp) and natural sunlight, with experiments conducted at different times of the year to account for seasonal variations.

The mechanism of the photo-oxidation reaction, shown in Figure 7, has been extensively studied [10,17,18]. It involves the activation of molecular oxygen ($^3O_2$) through the light excitation (*hν*) of a photosensitizer (*Sens*). The generated singlet oxygen ($^1O_2$) binds

to the furan ring and facilitates the formation of an endoperoxide intermediate, which subsequently leads to the production of 5-hydroxy-2(5H)-furanone. The presence of alcohol in the reaction medium enhances this mechanism. Notably, the 5% MeOH content does not alter the swelling, adsorption, or stability properties of the microgel. Control experiments were performed in the dark and with free Rose Bengal in a 0.011 M solution, equivalent to the concentration of RB anchored to the microgel.

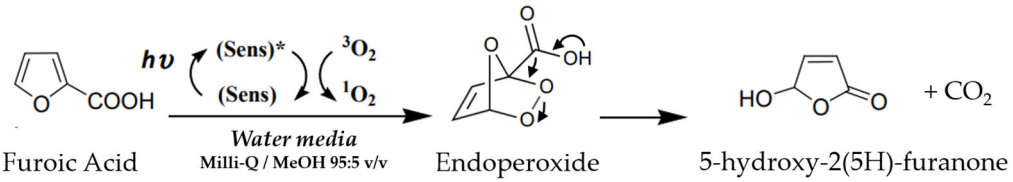


**Figure 7.** Reaction pathway for the photo-oxidation of 2-furoic acid to 5-hydroxy-2(5H)-furanone via singlet oxygen. Photosensitizer (Sens) transitions to its excited singlet state (Sens*) after sun irradiation (hυ), generating singlet oxygen ($^1O_2$) from ground-state molecular oxygen ($^3O_2$.). The process involves the formation of an endoperoxide intermediate.

Table 4 presents the kinetic parameters for the different irradiation scenarios, showing that the supported photocatalyst achieved complete conversion of furoic acid to 5-hydroxy-2(5H)-furanone in approximately 7 h of reaction time in all cases. Additionally, product characterization studies performed by HPLC chromatography confirm a pure conversion to 5-hydroxy-2(5H)-furanone, with no remaining reactants or byproducts detected, such as further oxidation to maleic acid or other compounds.

**Table 4.** Kinetic parameters and conversion rates (t = 420 min) for furoic acid photo-oxidation using heterogenous or homogeneous photosensitizers in different irradiation scenarios.

| Photosensitizer | | Conversion of Furoic Acid at t = 420 min | t ½ (min) | $k_{obs}$ ($min^{-1}$) |
|---|---|---|---|---|
| Halogen lamp Irradiation = 6.9 kWh/$m^2$ | Blank | - | - | - |
| | NIPAM-co-AEMA | - | - | - |
| | NIPAM-co-AEMA-RB | >99% | 61 | 0.01143 |
| | RB | 12% | 2277 | 0.00030 |
| June sunlight Irradiation = 7.5 kWh/$m^2$ | Blank | - | - | - |
| | NIPAM-co-AEMA | - | - | - |
| | NIPAM-co-AEMA-RB | >99% | 60 | 0.01140 |
| | RB | 13% | 2090 | 0.00033 |
| September sunlight Irradiation = 6.1 kWh/$m^2$ | Blank | - | - | - |
| | NIPAM-co-AEMA | - | - | - |
| | NIPAM-co-AEMA-RB | >99% | 61 | 0.01134 |
| | RB | | 2498 | 0.00028 |
| December sunlight Irradiation = 2.9 kWh/$m^2$ | Blank | - | - | - |
| | NIPAM-co-AEMA | - | - | - |
| | NIPAM-co-AEMA-RB | 98% | 74 | 0.00931 |
| | RB | 9% | 3087 | 0.00022 |

In this case, the performance difference between free RB and microgel-supported RB is significantly more pronounced than with the previous substrates. The heterogeneous photocatalyst NIPAM-co-AEMA-RB demonstrated enhanced efficiency due to the adsorption properties of the microgel. According to the literature, this reaction with free RB is only effective in alcohol-based media and fails to proceed in aqueous environments [10,18]. The notably low reaction kinetics observed for free RB further confirm the importance of the adsorption effect provided by the microgel. The use of heterogeneous catalysis and the adsorption effect of the microgel allowed for kinetic parameters in aqueous media that are

comparable to those reported in previous studies conducted in 100% MeOH [17]. This result underscores the sustainable design and efficiency of this system. The local concentration effect facilitated the interaction between the substrate, the covalently anchored RB, and the MeOH in the system, possibly due to the formation of a micelle-like structure, as described in the literature [36].

Within the first hour of reaction, the heterogeneous photocatalyst achieves approximately 50% 5-hydroxy-2(5H)-furanone conversion. Figure 8 depicts the kinetic profiles for the formation of the product under the four irradiation conditions studied. In December, a slightly longer time is required to reach >99% conversion (430 min), likely due to the lower average irradiation resulting from shorter daylight hours and the prolonged reaction duration.

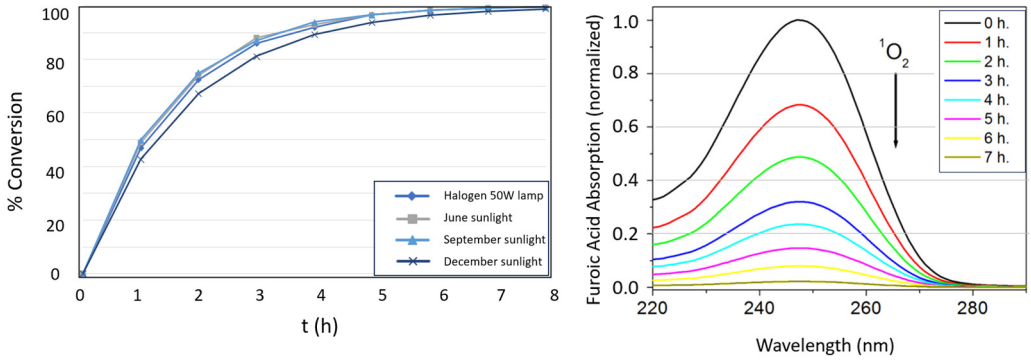


**Figure 8.** (**Left**) Conversion ratio of 5-hydroxy-2(5H)-furanone as a function of time under different irradiation scenarios. (**Right**) Evolution of the absorption band (λ = 246 nm) of furoic acid as a function of time under the December solar irradiation scenario, in both cases for NIPAM-co-AEMA-RB.

Recyclability studies were carried out during a period of moderate solar irradiation (September and October), spanning 25 complete cycles, equivalent to 175 h of total irradiation. Due to the limitation of sunlight, each cycle was conducted on a different day, with each reaction lasting 7 h. Notably, after 25 cycles, the NIPAM-co-AEMA-RB photocatalyst maintained its catalytic performance without any measurable loss of activity. On the other hand, the reaction demonstrates remarkable efficiency, achieving a high yield with excellent atomic economy, fully aligned with the principles of green chemistry and generating practically no byproducts. The $CO_2$ released during the process could be captured using an additional adsorption system, further enhancing its sustainability. Based on the catalytic performance and the mass balance of the 5-hydroxy-2(5H)-furanone synthesis, it is notable that, under the studied conditions—representing a TRL of 4–5 and still far from industrial-scale operations—the 500 mL jacketed reactor, with a $1 \times 10^{-3}$ M concentration of furoic acid, produces approximately 50 g of 5-hydroxy-2(5H)-furanone per cycle (1.25 kg of product in the 25 cycles studied).

### *3.5. Energy and Cost-Effective Calculations for Industrial Scale-Up*

The energy OPEX calculations for the two proposed systems—emerging contaminant removal and the green synthesis of 5-hydroxy-2(5H)-furanone—were conducted. Energy consumption for both processes was analyzed under two scenarios: halogen lamp irradiation and natural solar irradiation. The calculations were based on the average energy consumption per reaction cycle, determined from a minimum of 20 experiments for each scenario. Seasonal variations were also considered for the solar irradiation experiments. The energy consumption was calculated by multiplying the reaction time per cycle (approximately 3 h for Diclofenac degradation and 7 h for the synthesis of 5-hydroxy-2(5H)-furanone) by the power requirements of the equipment used. This included a 50 W

lamp (excluded for solar irradiation experiments), a 5 W stirring system, temperature and solar irradiation sensors with a combined power of 8 W, a 1060 W heater (only taken into account for the active heating time during each experiment), and a centrifuge, operated for 12 min at the end of each cycle to recover the photocatalyst. The results presented in Table 5 reveal a lower energy consumption for Diclofenac degradation compared to furoic acid oxidation, attributed to the longer reaction time required per cycle in the latter process. Importantly, energy consumption under lamp irradiation is more than twice that of direct solar irradiation for both scenarios. This underscores the significant impact of the lamp on overall energy usage. Substituting lamp irradiation with direct sunlight greatly improves the cost-effectiveness and enhances the economic and environmental sustainability of the process.

**Table 5.** Energy consumption across different reactor scales for Diclofenac degradation and furoic acid oxidation under halogen lamp and sunlight conditions. Scale-up comparison using the Aspen and Six-Tenths Rule methods (detailed calculations provided in the Supplementary Materials).

| Process | Energy Consumption ($kWh/m^3$) Reactor 500 mL | Reactor Scale-Up 1 $m^3$. Energy Consp. ($kWh/m^3$) | | Reactor Scale-Up 100 $m^3$. Energy Consp. ($kWh/m^3$) | | Reactor Scale-Up 1 $Hm^3$. Energy Consp. ($kWh/m^3$) | |
|---|---|---|---|---|---|---|---|
| | | Aspen | Six-Tenths | Aspen | Six-Tenths | Aspen | Six-Tenths |
| Diclofenac (halogen lamp) | 537 | 24.38 | 25.69 | 4.12 | 4.07 | 0.27 | 0.26 |
| Diclofenac (sunlight) | 253 | 12.48 | 12.09 | 2.01 | 1.92 | 0.12 | 0.12 |
| Furoic Acid (halogen lamp) | 1050 | 48.36 | 50.21 | 7.85 | 7.96 | 0.48 | 0.50 |
| Furoic Acid (sunlight) | 375 | 18.05 | 17.95 | 2.92 | 2.85 | 0.17 | 0.18 |

As detailed in the table, an energy OPEX cost analysis was performed at an economy-of-scale level to assess energy consumption per unit of treated volume. Two approaches were employed in this study to validate the extrapolated results. One method involved the use of the Aspen Process Economic Analyzer tool (version 14), a well-established software widely recognized for its accuracy in estimating economy-of-scale costs from real chemical process data and its effectiveness in calculating operational expenses, including energy OPEX. The Rule of Six-Tenths, a widely recognized method in chemical engineering for estimating both CAPEX and OPEX costs across different scales, was also applied [60–63]. The results obtained from both approaches are closely aligned, demonstrating a clear and expected trend: as the treatment volume increases, the energy consumption per unit volume ($kWh/m^3$) decreases. For instance, at a TRL 6–7 scale with a reactor volume of 1 $m^3$, the energy OPEX for sunlight-driven treatments is approximately 12 $kWh/m^3$ for Diclofenac and 18 $kWh/m^3$ for furoic acid, which is notably lower than the energy consumption observed for the 500 mL experimental reactor at TRL 4–5. In an industrial-scale scenario, such as a treatment plant with a capacity of one hectometer cubed of water, the energy consumption further decreases to approximately 0.1–0.2 $kWh/m^3$ treated, representing a highly competitive energy demand for a water purification process [64].

Within the principles of green chemistry, the reactor operates without requiring any additional chemical compounds beyond the microgels. Furthermore, the natural pH of the microgels closely aligns with that of wastewater effluents from WWTPs, making the system

well suited for integration as an advanced tertiary or quaternary treatment in current water disinfection processes.

Nevertheless, the implementation of this technology at an industrial scale in WWTPs faces challenges related to scalability, photocatalytic efficiency, and material recovery. Large-scale production must ensure a reproducible and economically viable synthesis of the microgels while maintaining their colloidal properties and the stability of the photosensitizer. The process efficiency depends on factors such as solar irradiation, substrate adsorption, and wastewater pH, which can be influenced by the presence of impurities and variations in environmental conditions. While the use of direct sunlight for industrial-scale applications poses challenges—such as the spectral distribution of solar photons, interruptions due to the day/night cycle, and weather variability [45]—the proposed system can be designed for flexibility. It can utilize both solar and artificial light sources, with a preference for sunlight to enhance sustainability, while artificial light serves as a reliable alternative when sunlight is unavailable. Moreover, the recovery and reuse of the microgels require efficient separation strategies that do not compromise catalytic activity over multiple cycles. It is essential to develop effective separation methods, assess the biodegradability and environmental safety of the materials, and ensure compliance with current environmental regulations. Market acceptance will depend on the evidence of its effectiveness in future large-scale TRL studies, particularly in the optimization and implementation of the process in an operational WWTP environment, as well as specific studies on material recyclability and stability. Additionally, further research should support its positive impact on the sustainability of wastewater treatment processes and the development of LCA and LCC studies.

Regarding environmental scalability, to ensure that the microgels do not generate secondary pollution after use, it is essential to evaluate their stability, degradability, and toxicity in aquatic environments. Strategies for their recovery and reuse will be developed in futures studies in order to minimize their release into the environment and prevent the formation of persistent nanoplastics. Additionally, it is crucial to analyze their potential ecotoxicological impact and the release of byproducts, ensuring they do not negatively affect aquatic organisms or accumulate in ecosystems. Future research will optimize their formulation to enhance environmental compatibility and assess their behavior under real conditions, ensuring compliance with regulations and the sustainable application of this technology in water treatment.

## 4. Conclusions

The microgels, designed following green chemistry principles, utilize a PNIPAM-based polymeric matrix with covalently anchored Rose Bengal, exhibiting properties to enhance substrate adsorption, reaction efficiency, and environmental sustainability. Their design supports sunlight-driven photocatalysis and sustainable applications in water treatment, achieving high polymerization efficiency, minimal waste, and reusability across multiple cycles. By using molecular oxygen from air as the oxidant and sunlight as the energy source, photocatalysis aligns with green chemistry principles, eliminating chemical oxidants and reducing energy barriers, thereby ensuring both environmental and economic benefits. NIPAM-co-AEMA-RB demonstrated effective adsorption properties for ADPA, Diclofenac, and furoic acid, attributed to its stimuli-responsive colloidal structure, which facilitates substrate adsorption. The reaction kinetics were superior to those of free RB, driven by the local concentration effect enabled by the polymeric matrix's colloidal structure at the reaction temperature. NIPAM-co-AEMA-RB achieved complete Diclofenac degradation in approximately 3 h and the synthesis of 5-hydroxy-2(5H)-furanone within 7 h. Recyclability studies demonstrated photosensitizer stability, maintaining kinetic properties over 25 cycles

in 2-furoic acid photo-oxidation, 40 cycles in Diclofenac degradation, and 100 cycles in ADPA oxidation. The microgel's adsorption properties enabled the synthesis of 5-hydroxy-2(5H)-furanone in aqueous media using the supported photocatalyst, contrasting with free RB and previous studies requiring alcohol-based solvents. This achievement, along with the demonstration that the technology is viable under direct solar irradiation conditions, represents the main novelty compared to previous studies, enhancing its scalability potential and underscoring the sustainable design of these materials, facilitating green catalytic reactions in water. Industrial-scale studies of the proposed system estimate energy consumption at 0.1–0.2 $kWh/m^3$ for direct solar-driven reactions, confirming its energy efficiency and sustainability in water treatment applications. The large-scale implementation of microgels in WWTPs presents challenges related to efficient separation, recyclability, and photocatalytic efficiency, and compliance with environmental regulations is crucial to prevent secondary pollution. Future research should explore the photo-oxidative potential of these microgels for other environmentally relevant reactions, investigate the degradation of additional CECs, and innovate in the field of polymeric structure design and substrate adsorption properties. Additionally, it will focus on optimizing material stability, ensuring sustainable integration into WWTPs through LCA and LCC studies and validating long-term viability under real operational conditions.

**Supplementary Materials:** The following supporting information can be downloaded at: https://www.mdpi.com/article/10.3390/su17052331/s1, Characterization Titrations: characterization of the amount of AEMA in polymer matrix and RB bounding calculation in NIPAM-co-AEMA-RB (in pdf and excel). Energy calculations: calculations of energy consumption in the processes and assessments for energy-OPEX scale-up studies (in pdf and excel).

**Author Contributions:** Conceptualization, V.F.; methodology, V.F.; formal analysis, V.F. and J.M.P.; investigation, V.F.; data curation, J.M.P.; writing—original draft, J.M.P.; writing—review and editing, V.F.; project administration, V.F. All authors have read and agreed to the published version of the manuscript.

**Funding:** This research was funded by the European Commission, Horizon 2020 research and innovation program under grant agreement No. 101036838, "Territorial Circular Systemic Solution for the Upcycling of Residues from the Agrifood Sector (Agro2Circular)".

**Data Availability Statement:** Data are contained within the article.

**Acknowledgments:** The authors wish to express their gratitude to Regenera Energy.

**Conflicts of Interest:** Both authors are employed by the company Regenera Energy.

## Abbreviations

The following abbreviations are used in this manuscript (ranked in order of appearance):

| | |
|---|---|
| CECs | Contaminants of Emerging Concern |
| WWTPs | Wastewater treatment plants |
| PNIPAM | Poly(N-isopropylacrylamide) |
| RB | Rose Bengal |
| EPs | Emerging pollutants |
| ADPA | 9,10-anthracenedipropionic acid |
| DLS | Dynamic light scattering |
| UV-Vis | Ultraviolet-visible spectroscopy |

| | |
|---|---|
| HPLC | High-Performance Liquid Chromatography |
| NIPAM | N-isopropylacrylamide |
| AEMA | Aminoethyl methacrylate |
| MBAM | N,N′-methylenebisacrylamide |
| EDC | 1-[3-(dimethylamino)propyl]-3-ethylcarbodiimide |
| MeOH | Methanol |
| t ½ | Half-reaction time |
| $k_{obs}$ | Observed rate constant or observed k |
| ($O_2(^1\Delta g)$) or $^1O_2$ | Singlet oxygen |
| $^3O_2$ | Molecular oxygen |
| *hv* | Light excitation or photon energy |
| TRL | Technology Readiness Level |
| CAPEX | Capital Expenditure |
| OPEX | Operational Expenditure |

## References


1. Anastas, P.T.; Warner, J.C. *Green Chemistry: Theory and Practice*; Oxford University Press: Oxford, UK, 2000.
2. Andraos, J.; Matlack, A.S. *Introduction to Green Chemistry*; CRC Press: Boca Raton, FL, USA, 2022.
3. Ncube, A.; Mtetwa, S.; Bukhari, M.; Fiorentino, G.; Passaro, R. Circular economy and green chemistry: The need for radical innovative approaches in the design for new products. *Energies* **2022**, *16*, 1752. [CrossRef]
4. Zuin, V.G.; Eilks, I.; Elschami, M.; Kümmerer, K. Education in green chemistry and in sustainable chemistry: Perspectives towards sustainability. *Green Chem.* **2021**, *23*, 1594–1608. [CrossRef]
5. Rout, P.R.; Zhang, T.C.; Bhunia, P.; Surampalli, R.Y. Treatment technologies for emerging contaminants in wastewater treatment plants: A review. *Sci. Total Environ.* **2021**, *753*, 141990. [CrossRef] [PubMed]
6. Morin-Crini, N.; Lichtfouse, E.; Liu, G.; Balaram, V.; Ribeiro, A.R.L.; Lu, Z.; Crini, G. Worldwide cases of water pollution by emerging contaminants: A review. *Environ. Chem. Lett.* **2022**, *20*, 2311–2338. [CrossRef]
7. Arman, N.Z.; Salmiati, S.; Aris, A.; Salim, M.R.; Nazifa, T.H.; Muhamad, M.S.; Marpongahtun, M. A review on emerging pollutants in the water environment: Existences, health effects and treatment processes. *Water* **2021**, *13*, 3258. [CrossRef]
8. Patel, N.A.V.E.E.N.; Khan, M.D.; Shahane, S.; Rai, D.; Chauhan, D.; Kant, C.; Chaudhary, V.K. Emerging pollutants in aquatic environment: Source, effect, and challenges in biomonitoring and bioremediation-a review. *Pollution* **2020**, *6*, 99–113.
9. Shahid, M.K.; Kashif, A.; Fuwad, A.; Choi, Y. Current advances in treatment technologies for removal of emerging contaminants from water–A critical review. *Coord. Chem. Rev.* **2021**, *442*, 213993. [CrossRef]
10. Zhang, Q.; Gu, B.; Fang, W. Sunlight-driven photocatalytic conversion of furfural and its derivatives. *Green Chem.* **2024**, *26*, 6261. [CrossRef]
11. Wu, X.; Luo, N.; Xie, S.; Zhang, H.; Zhang, Q.; Wang, F.; Wang, Y. Photocatalytic transformations of lignocellulosic biomass into chemicals. *Chem. Soc. Rev.* **2020**, *49*, 6198–6223. [CrossRef]
12. Wang, M.; Wang, F. Catalytic scissoring of lignin into aryl monomers. *Adv. Mater.* **2019**, *31*, 1901866. [CrossRef]
13. Li, C.; Zhao, X.; Wang, A.; Huber, G.W.; Zhang, T. Catalytic transformation of lignin for the production of chemicals and fuels. *Chem. Rev.* **2015**, *115*, 11559–11624. [CrossRef] [PubMed]
14. Mariscal, R.; Maireles-Torres, P.; Ojeda, M.; Sádaba, I.; Granados, M.L. Furfural: A renewable and versatile platform molecule for the synthesis of chemicals and fuels. *Energy Environ. Sci.* **2016**, *9*, 1144–1189. [CrossRef]
15. van Putten, R.J.; Van Der Waal, J.C.; De Jong, E.D.; Rasrendra, C.B.; Heeres, H.J.; de Vries, J.G. Hydroxymethylfurfural, a versatile platform chemical made from renewable resources. *Chem. Rev.* **2013**, *113*, 1499–1597. [CrossRef] [PubMed]
16. Bozell, J.J.; Petersen, G.R. Technology development for the production of biobased products from biorefinery carbohydrates—The US Department of Energy's "Top 10" revisited. *Green Chem.* **2010**, *12*, 539–554. [CrossRef]
17. Fabregat, V.; Burguete, M.I.; Galindo, F. Singlet oxygen generation by photoactive polymeric microparticles with enhanced aqueous compatibility. *Environ. Sci. Pollut. Res.* **2014**, *21*, 11884–11892. [CrossRef]
18. Huang, Y.M.; Lu, G.H.; Zong, M.H.; Cui, W.J.; Li, N. A plug-and-play chemobiocatalytic route for the one-pot controllable synthesis of biobased C4 chemicals from furfural. *Green Chem.* **2021**, *23*, 8604–8610. [CrossRef]
19. Xu, C.; Paone, E.; Rodríguez-Padrón, D.; Luque, R.; Mauriello, F. Recent catalytic routes for the preparation and the upgrading of biomass derived furfural and 5-hydroxymethylfurfural. *Chem. Soc. Rev.* **2020**, *49*, 4273–4306. [CrossRef]
20. Saunders, B.R.; Vincent, B. Microgel particles as model colloids: Theory, properties and applications. *Adv. Colloid Interface Sci.* **1999**, *80*, 1–25. [CrossRef]

21. Trombino, S.; Sole, R.; Di Gioia, M.L.; Procopio, D.; Curcio, F.; Cassano, R. Green chemistry principles for nano and micro-sized hydrogel synthesis. *Molecules* **2023**, *28*, 2107. [CrossRef]
22. Rozhkova, Y.A.; Burin, D.A.; Galkin, S.V.; Yang, H. Review of microgels for enhanced oil recovery: Properties and cases of application. *Gels* **2022**, *8*, 112. [CrossRef]
23. Das, A.; Babu, A.; Chakraborty, S.; Van Guyse, J.F.; Hoogenboom, R.; Maji, S. Poly (N-isopropylacrylamide) and Its Copolymers: A Review on Recent Advances in the Areas of Sensing and Biosensing. *Adv. Funct. Mater.* **2024**, *34*, 2402432. [CrossRef]
24. Guerron, A.; Giasson, S. Multiresponsive microgels: Toward an independent tuning of swelling and surface properties. *Langmuir* **2021**, *37*, 11212–11221. [CrossRef] [PubMed]
25. Gopalakrishnan, G.; Jeyakumar, R.B.; Somanathan, A. Challenges and emerging trends in advanced oxidation technologies and integration of advanced oxidation processes with biological processes for wastewater treatment. *Sustainability* **2023**, *15*, 4235. [CrossRef]
26. Sheldon, R.A.; Brady, D. Green chemistry, biocatalysis, and the chemical industry of the future. *ChemSusChem* **2022**, *15*, e202102628. [CrossRef]
27. Marin, M.L.; Santos-Juanes, L.; Arques, A.; Amat, A.M.; Miranda, M.A. Organic photocatalysts for the oxidation of pollutants and model compounds. *Chem. Rev.* **2012**, *112*, 1710–1750. [CrossRef]
28. Ravelli, D.; Dondi, D.; Fagnoni, M.; Albini, A. Photocatalysis. A multi-faceted concept for green chemistry. *Chem. Soc. Rev.* **2009**, *38*, 1999–2011. [CrossRef]
29. Ghogare, A.A.; Greer, A. Using singlet oxygen to synthesize natural products and drugs. *Chem. Rev.* **2016**, *116*, 9994–10034. [CrossRef]
30. Al-Nu'airat, J.; Oluwoye, I.; Zeinali, N.; Altarawneh, M.; Dlugogorski, B.Z. Review of chemical reactivity of singlet oxygen with organic fuels and contaminants. *Chem. Rec.* **2021**, *21*, 315–342. [CrossRef]
31. Fabregat, V. Enhancing Emerging Pollutant Removal in Industrial Wastewater: Validation of a Photocatalysis Technology in Agri-Food Industry Effluents. *Appl. Sci.* **2024**, *14*, 6308. [CrossRef]
32. Fabregat, V. Exploring the Role of pH and Solar Light-Driven Decontamination with Singlet Oxygen in Removing Emerging Pollutants from Agri-Food Effluents: The Case of Acetamiprid. *Physchem* **2025**, *5*, 9. [CrossRef]
33. Koizumi, H.; Shiraishi, Y.; Tojo, S.; Fujitsuka, M.; Majima, T.; Hirai, T. Temperature-driven oxygenation rate control by polymeric photosensitizer. *J. Am. Chem. Soc.* **2006**, *128*, 8751–8753. [CrossRef] [PubMed]
34. Shiraishi, Y.; Suzuki, T.; Hirai, T. Temperature-and pH-responsive photosensitization activity of polymeric sensitizers based on poly-N-isopropylacrylamide. *Polymer* **2009**, *50*, 5758–5764. [CrossRef]
35. Shiraishi, Y.; Kimata, Y.; Koizumi, H.; Hirai, T. Temperature-controlled photooxygenation with polymer nanocapsules encapsulating an organic photosensitizer. *Langmuir* **2008**, *24*, 9832–9836. [CrossRef] [PubMed]
36. Koizumi, H.; Kimata, Y.; Shiraishi, Y.; Hirai, T. Temperature-controlled changeable oxygenation selectivity by singlet oxygen with a polymeric photosensitizer. *Chem. Commun.* **2007**, *18*, 1846–1848. [CrossRef] [PubMed]
37. Egil, A.C.; Carmignani, A.; Battaglini, M.; Sengul, B.S.; Acar, E.; Ciofani, G.; Ince, G.O. Dual stimuli-responsive nanocarriers via a facile batch emulsion method for controlled release of Rose Bengal. *J. Drug Deliv. Sci. Technol.* **2022**, *74*, 103547. [CrossRef]
38. Don, T.M.; Lu, K.Y.; Lin, L.J.; Hsu, C.H.; Wu, J.Y.; Mi, F.L. Temperature/pH/Enzyme triple-responsive cationic protein/PAA-b-PNIPAAm nanogels for controlled anticancer drug and photosensitizer delivery against multidrug resistant breast cancer cells. *Mol. Pharm.* **2017**, *14*, 4648–4660. [CrossRef]
39. Maki, Y.; Dobashi, T. Poly (N-isopropylacrylamide)-clay nanocomposite hydrogels with patterned thermo-responsive behavior. *Trans. Mater. Res. Soc. Jpn.* **2017**, *42*, 119–122. [CrossRef]
40. Nowakowska, M.; Kępczyński, M.; Dąbrowska, M. Polymeric Photosensitizers, 5. Synthesis and Photochemical Properties of Poly [(N-isopropylacrylamide)-co-(vinylbenzyl chloride)] Containing Covalently Bound Rose Bengal Chromophores. *Macromol. Chem. Phys.* **2001**, *202*, 1679–1688. [CrossRef]
41. Nowakowska, M.; Kepczynski, M.; Szczubialka, K. New polymeric photosensitizers. *Pure Appl. Chem.* **2001**, *73*, 491–495. [CrossRef]
42. Nowakowska, M.; Szczubiałka, K. Photoactive polymeric and hybrid systems for photocatalytic degradation of water pollutants. *Polym. Degrad. Stab.* **2017**, *145*, 120–141. [CrossRef]
43. Blázquez-Moraleja, A.; Moya, P.; Marin, M.L.; Bosca, F. Synthesis of novel heterogeneous photocatalysts based on Rose Bengal for effective wastewater disinfection and decontamination. *Catal. Today* **2023**, *413*, 113948. [CrossRef]
44. Flores, J.; Moya, P.; Bosca, F.; Marin, M.L. Photoreactivity of new rose bengal-SiO2 heterogeneous photocatalysts with and without a magnetite core for drug degradation and disinfection. *Catal. Today* **2023**, *413*, 113994. [CrossRef]
45. Esser, P.; Pohlmann, B.; Scharf, H.D. The photochemical synthesis of fine chemicals with sunlight. *Angew. Chem. Int. Ed. Engl.* **1994**, *33*, 2009–2023. [CrossRef]
46. Roy, J.S.; Messaddeq, Y. The Role of Solar Concentrators in Photocatalytic Wastewater Treatment. *Energies* **2024**, *17*, 4001. [CrossRef]

47. Saravanan, A.; Kumar, P.S.; Vo, D.V.N.; Yaashikaa, P.R.; Karishma, S.; Jeevanantham, S.; Bharathi, V.D. Photocatalysis for removal of environmental pollutants and fuel production: A review. *Environ. Chem. Lett.* **2021**, *19*, 441–463. [CrossRef]
48. Xie, Y.; Jiang, Q.; Zhang, Y.; Zhang, K.; Hou, J.; Feng, M. Recent advances in solar-enhanced homogeneous water decontamination and disinfection: A review. *Sep. Purif. Technol.* **2023**, *325*, 124678. [CrossRef]
49. Lee, B.C.Y.; Lim, F.Y.; Loh, W.H.; Ong, S.L.; Hu, J. Emerging contaminants: An overview of recent trends for their treatment and management using light-driven processes. *Water* **2021**, *13*, 2340. [CrossRef]
50. Fabregat, V.; Burguete, M.I.; Luis, S.V.; Galindo, F. Improving photocatalytic oxygenation mediated by polymer supported photosensitizers using semiconductor quantum dots as 'light antennas'. *RSC Adv.* **2017**, *7*, 35154–35158. [CrossRef]
51. Burguete, M.I.; Fabregat, V.; Galindo, F.; Izquierdo, M.A.; Luis, S.V. Improved polyHEMA–DAQ films for the optical analysis of nitrite. *Eur. Polym. J.* **2009**, *45*, 1516–1523. [CrossRef]
52. Fabregat, V.; Izquierdo, M.A.; Burguete, M.I.; Galindo, F.; Luis, S.V. Quantum dot–polymethacrylate composites for the analysis of NOx by fluorescence spectroscopy. *Inorganica Chim. Acta* **2012**, *381*, 212–217. [CrossRef]
53. Fabregat, V.; Izquierdo, M.Á.; Burguete, M.I.; Galindo, F.; Luis, S.V. Nitric oxide sensitive fluorescent polymeric hydrogels showing negligible interference by dehydroascorbic acid. *Eur. Polym. J.* **2014**, *55*, 108–113. [CrossRef]
54. Fabregat, V.; Burguete, M.I.; Galindo, F.; Luis, S.V. Influence of polymer composition on the sensitivity towards nitrite and nitric oxide of colorimetric disposable test strips. *Environ. Sci. Pollut. Res.* **2017**, *24*, 3448–3455. [CrossRef] [PubMed]
55. Bradley, M.; Vincent, B. Poly (vinylpyridine) core/poly (N-isopropylacrylamide) shell microgel particles: Their characterization and the uptake and release of an anionic surfactant. *Langmuir* **2008**, *24*, 2421–2425. [CrossRef] [PubMed]
56. Bradley, M.; Vincent, B.; Burnett, G. Uptake and Release of Anionic Surfactant into and from Cationic Core− Shell Microgel Particles. *Langmuir* **2007**, *23*, 9237–9241. [CrossRef] [PubMed]
57. Burakowska, E.; Zimmerman, S.C.; Haag, R. Photoresponsive crosslinked hyperbranched polyglycerols as smart nanocarriers for guest binding and controlled release. *Small* **2009**, *5*, 2199–2204. [CrossRef]
58. Atkins, P.W.; De Paula, J.; Keeler, J. *Atkins' Physical Chemistry*; Oxford University Press: Oxford, UK, 2023.
59. Available online: https://www.aemet.es/documentos/es/serviciosclimaticos/datosclimatologicos/atlas_radiacion_solar/atlas_de_radiacion_24042012.pdf (accessed on 12 January 2025).
60. Peters, M.S.; Timmerhaus, K.D.; West, R.E. *Plant Design and Economics for Chemical Engineers*, 5th ed.; McGraw-Hill: New York, NY, USA, 2003; Volume 66.
61. Mahmud, R.; Moni, S.M.; High, K.; Carbajales-Dale, M. Integration of techno-economic analysis and life cycle assessment for sustainable process design–A review. *J. Clean. Prod.* **2021**, *317*, 128247. [CrossRef]
62. Zagklis, D.P.; Papageorgiou, C.S.; Paraskeva, C.A. Technoeconomic analysis of the recovery of phenols from olive mill wastewater through membrane filtration and resin adsorption/desorption. *Sustainability* **2021**, *13*, 2376. [CrossRef]
63. Fabregat, V.; Pagán, J.M. Technical–Economic Feasibility of a New Method of Adsorbent Materials and Advanced Oxidation Techniques to Remove Emerging Pollutants in Treated Wastewater. *Water* **2024**, *16*, 814. [CrossRef]
64. Dirección General del Agua, Ministerio para la Transición Ecológica y el Reto Demográfico. *Mejora de la Eficiencia Energética e Integral de las Plantas de Tratamiento, Regeneración y Reutilización de Aguas Residuales—Informe Complementario*; Dirección General del Agua, Ministerio para la Transición Ecológica y el Reto Demográfico: Madrid, Spain, 2020.


**Disclaimer/Publisher's Note:** The statements, opinions and data contained in all publications are solely those of the individual author(s) and contributor(s) and not of MDPI and/or the editor(s). MDPI and/or the editor(s) disclaim responsibility for any injury to people or property resulting from any ideas, methods, instructions or products referred to in the content.